THE JOURNAL OF PHYSICAL CHEMISTRY C LETTERS

2009, *113,* 9018–9022
Published on Web 05/05/2009

Revealing Quantitative 3D Chemical Arrangement on Ge−Si Nanostructures

Luciano A. Montoro,[†] Marina S. Leite,[†] Daniel Biggemann,[†] Fellipe G. Peternella,[†] K. Joost Batenburg,[§] Gilberto Medeiros-Ribeiro,[†,‡] and Antonio J. Ramirez*,[†]

Brazilian Synchrotron Light Laboratory, Caixa Postal 6192, Campinas SP 13083-970, Brazil, Hewlett-Packard Laboratories, P.O. Box 10350, Palo Alto, California 94303-0867, U.S.A., and University of Antwerp, Universiteitsplein 1, B-2610, Wilrijk, Belgium

Received: March 19, 2009; Revised Manuscript Received: April 25, 2009

The knowledge of composition and strain with atomic resolution is of utmost importance for the understanding of the chemical and electronic properties of alloyed nanostructures, and they can only be extracted in a self-consistent fashion. As an example, several works have addressed the issue of strain and chemical composition on self-assembled epitaxial islands using different techniques such as X-ray diffraction, scanning probe microscopy and transmission electron microscopy (TEM). However, limited information is available on the 3D chemical composition of such nanostructures. Here, we demonstrate the use of a quantitative high-resolution transmission electron microscopy (QHRTEM) technique to obtain two-dimensional (2D) projected chemical maps of epitaxially grown Ge−Si/Si(001) islands, with high spatial resolution, at different crystallographic orientations. Combining these data with iterative simulation, the reconstruction of the three-dimensional (3D) chemical arrangement on the strained Ge−Si/Si(001) islands was realized. This methodology can be applied for a large variety of strained crystalline systems, such as nanowires, epitaxial islands, quantum dots and wells, and partially relaxed heterostructures.

In recent years, intensive efforts have been dedicated to the development of nanoscale 3D imaging techniques.[1−5] Electron tomography methodologies employing bright field TEM, HAADF-scanning transmission electron microscopy (STEM), or energy-filtered TEM typically require a large and angle-comprehensive tilt series of projections for a 3D reconstruction, providing morphological features with spatial resolution down to 1 nm[3] and restricted chemical information.[1,2] Some pioneering work on STEM coupled with image simulation,[3] Cs-corrected TEM,[4] and discrete tomography based on high-resolution TEM[5] has made possible the 3D reconstruction of isolated nanocrystals, achieving atomic-scale resolution. However, the determination of quantitative 3D composition and structural data on alloyed nanostructures continues to be a challenge.

The investigation of zero-dimensional (quantum dots), one-dimensional (wires), and two-dimensional (thin layers) strained epitaxial structures in the past decades has produced an enormous variety of scientific results which can bear significant importance to new semiconductor devices. Of these low-dimensional systems, heteroepitaxial semiconductor islands have attracted a lot of attention primarily because of their optical and electronic properties.[6] Furthermore, they can serve as a model system that permits the understanding of structural properties and thermodynamics at the nanoscale.[7] For example, the control of shape, size, composition, and elastic strain of the islands resides on a delicate balance between kinetics and thermodynamics, which has important consequences on their use in electronic devices.[6] Ge−Si epitaxial islands have been by far the most extensively studied alloyed nanostructured system, using techniques such as atomic force microscopy (AFM) combined with selective chemical etching,[8] X-ray absorption fine structure,[9] TEM,[10,11] and grazing incidence anomalous X-ray diffraction (GIXRD).[12,13] All support the existence of vertical composition variations, with most of the Si at the base of the island and the Ge concentration increasing monotonically from the base to the top. Several growth methods and parameters leading to distinct kinetic conditions will produce different profiles, which further call for tools that can give a complete, unambiguous, and high-resolution picture of the composition. Energy-dispersive X-ray spectroscopy (XEDS) and electron energy loss spectroscopy (EELS) associated to STEM has been used to provide chemical profiles of individual islands.[11,14] However, the results obtained using these techniques have a limited spatial resolution and/or fail to provide information regarding the 3D composition distribution of the entire island.

On the other hand, additional information can be provided by QHRTEM techniques. In the past decade, several methods have been proposed and applied to different systems to obtain quantitative crystallographic information, strain/stress, and chemical composition from high-resolution TEM (HRTEM) images.[15] A useful method for strain and chemical composition analysis is based on lattice spacing measurement. For most binary ($A_{1-x}B_x$) and pseudobinary ($A_{1-x}B_xC$) alloys, Vegard's law assumes a linear relationship between the lattice parameter and the chemical composition. QHRTEM has been successfully

* To whom correspondence should be addressed. E-mail: ramirez@lnls.br. Phone: 55-19-3518-3108.
[†] Brazilian Synchrotron Light Laboratory.
[§] University of Antwerp.
[‡] Hewlett-Packard Laboratories.

applied to the investigation of semiconductor quantum well layers, incoherently III−V strained islands, and quantum dots.[15,16]

Here, we combine geometrical phase analysis (GPA)[17] and focal series aberration corrected images obtained by HRTEM at two orientations on 40 ± 5 nm diameter Ge_xSi_{1-x}/Si(001) islands, allowing the investigation of their 3D chemical composition in a quantitative fashion.

GPA is a method for measuring and mapping structural displacement fields on HRTEM images using a reference lattice. This analysis is based upon Fourier filtering of the image, providing geometrical phase information which is related to local distortions of atomic planes and consequently to the lattice parameters. This method has been effectively employed by Hÿtch et al.[18,19] to study strain fields with resolutions down to 0.001 nm in semiconductors and metals. Important aspects of the images considered for GPA are the absence of contrast reversals in the image through the sample thickness and the absence of significant delocalization contrast.[20] The thickness variation in ∼40 nm diameter Ge−Si islands did not cause contrast reversals at the used defocus.

The focal series reconstruction (FSR) is a numerical technique for the restoration of the phase and the amplitude of the exit plane wave function from a series of images obtained with different defocus values.[21] By this means, objective lens aberration-free images with improved resolution that nearly achieve the instrumental information limit can be obtained. This exit plane wave reconstruction procedure applied together with GPA improves the accuracy of the quantitative determination of the displacement fields, reducing the effect of the aberrations introduced by the microscope imaging system.[20,22] In addition, the minor distortions caused in the images by the TEM projector lenses, which could compromise the quantification of the displacement fields, have been corrected using a GPA-based procedure.[23]

This methodology has been applied to obtain the Ge−Si islands' distortion maps and, from them, their respective lattice parameter components (parallel, $a_{||}$ and perpendicular, $a_{\perp}$). Composition and strain component ($\varepsilon_{||}$ and $\varepsilon_{\perp}$) maps were determined in a self-consistent manner by relating the lattice parameters ($a_{||}$ and $a_{\perp}$) by anisotropic elastic theory using the composition-dependent stiffness coefficients, assuming biaxial stress and Vegard's law. Vegard's law has been verified for numerous alloys, exhibiting deviations below $\sim 2\%_{atom}$,[24,25] which are lower than the quantification limit imposed by GPA method (approximately 0.001 nm or 4.5% Ge for the Ge−Si system).[18] The biaxial stress state is usually adopted for thin film elastic modeling. However, it can be assumed as a valid approximation for small epitaxial islands. Molecular dynamics[26] and finite elements[27] simulation have shown that the average perpendicular stress is less than 5% of the average parallel stress. No further assumptions were utilized, allowing the use of this methodology in other alloyed systems with lattice mismatch. A detailed description of the procedure employed to calculate the chemical maps from displacement fields is presented in the Supporting Information (Theoretical Basis).

Ge−Si islands were grown on a Si(001)-oriented substrate by a chemical vapor deposition (CVD) technique at a total pressure of 1.3 kPa (10 Torr) in a lamp-heated single wafer reactor with a wafer supported by a SiC-coated graphite plate with moderate thermal mass. The temperature was measured by an optical pyrometer focused on the back of the support plate. An in situ surface preparation baking was conducted by heat treatment at about 1150 °C in a H_2 ambient to clean the surface. The temperature was then reduced to 1080 °C, and a Si buffer layer was deposited using SiH_2Cl_2 in a H_2 carrier gas. After depositing the buffer layer, the temperature was reduced to the Ge deposition temperature of 605 °C, and the Ge was deposited using GeH_4 with a partial pressure of 0.065 Pa in a H_2 carrier gas for 120 s, resulting in a final thickness of ∼12 equiv ML (1 equivalent monolayer = 6.27×10^{14} Ge atoms/cm^2). After the deposition ended, the wafer remained at the deposition temperature in a H_2 ambient for approximately 5 s while the reactant was purged from the system and subsequently cooled and then removed from the deposition chamber into a N_2 ambient.[28] AFM statistical analysis (not shown) pointed out uniform dome-shaped islands with a narrow size distribution.

TEM cross section specimens oriented at the [110] and [100] zone axis were prepared using manual and dimpler polishing followed by liquid-nitrogen-cooled Ar^+ ion beam thinning with energies of 3.5 and 2 keV at incidence angles gradually decreasing from 6 to 2°. A JEM-3010 URP TEM with a LaB_6 electron gun and spherical aberration coefficient of 0.7 mm was used at an accelerating voltage of 300 kV. The distortions introduced into HRTEM images by the projector lens system were removed using the procedure proposed by Hüe et al.[23] Spherical aberration corrected HRTEM images were obtained using exit plane wave function restoration from the focal series technique. The procedure used for the restoration was the Wiener filter method, implemented as a routine (FTSR from HREM Research Inc.) written for the software package Digital Micrograph.[21] Sets of images for focal series reconstruction were recorded on a 1024 × 1024 thermoelectrically cooled CCD camera with a focal step of 5 nm between exposures. An adequate magnification was chosen to obtain a sampling rate of ∼0.030 nm per pixel, that is, an image discretization well below the Nyquist limit of 0.077 nm, excluding aliasing phenomena. The image processing by the geometric phase analysis was carried out using a routine (GPA from HREM Research Inc.) implemented on Digital Micrograph[17] and was applied to the amplitude image obtained from the reconstructed exit wave. The exit wave amplitude was used for the analyses due to its lower thickness dependency when compared with that of the wave phase. For the GPA processing, a Lorentzian mask was used with a half-width of $1/4*d_{111}$ in reciprocal space, resulting in 2D chemical and strain maps with 1.6 nm spatial resolution. The GPA processing was comparatively performed using different reflections in the Fourier space, such as the {110} spot for [100] oriented specimen and {111} and {100} for [110] oriented ones. The strain and chemical maps were constructed based on the reflections with higher intensities, which provide a better signal-to-noise relation, resulting in better geometric phase resolution and compositional accuracy. The reference lattice used for the GPA analysis was an undistorted pure silicon region of the substrate far from the domes and the surface. The precision in the chemical quantification was estimated for each map based on the standard deviation of the measured composition in a Ge-free region of the silicon substrate.

Figure 1A−D shows the 2D strain and chemical maps of two representative islands obtained self-consistently from the high-resolution images of the reconstructed exit plane wave function amplitude along the [110] and [100] directions. The islands were partially mapped due to the CCD size limitation and the employed magnification, which provides adequate sampling. These strain and chemical maps are side-view projections of the islands, representing the values averaged through the atomic columns. A careful analysis of the chemical maps (not show) obtained from several islands in different TEM specimens

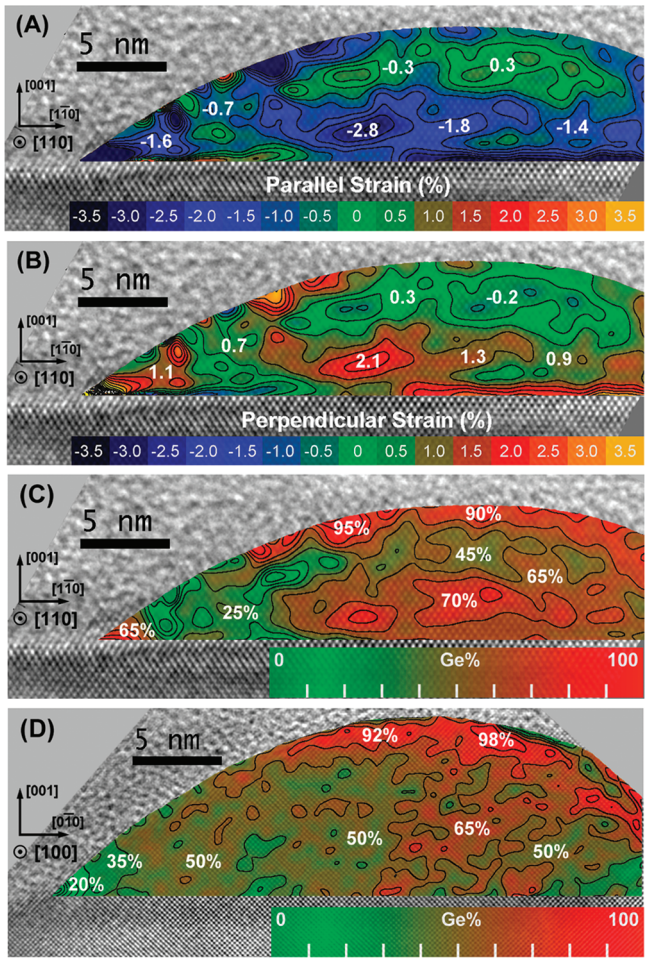

Figure 1. Two-dimensional strain and chemical maps of representative Ge−Si/Si(001) dome-shaped islands. (A and B) Strain maps obtained from the [110] projection, showing the parallel and perpendicular components ($\varepsilon_{\parallel}$ and $\varepsilon_{\perp}$), respectively. The color scale indicates the strain level, where the positive values correspond to an expansion of lattice and the negative values to contraction. (C and D) Chemical maps obtained along the [110] and [100] crystallographic directions, respectively. These maps show the average Ge content ($\%_{atom}$) at the projected directions, obtained from the quantitative high-resolution transmission electron microscopy technique. The color code indicates the Ge content. All maps are superposed to the original HRTEM images, showing the coherently strained Ge−Si islands on the Si(001) substrate.

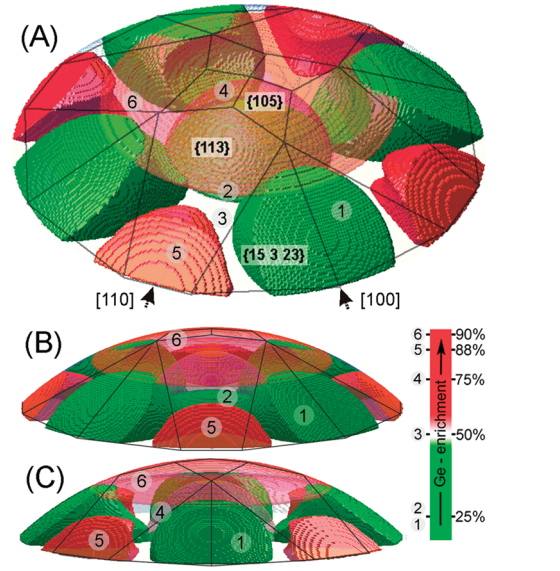

Figure 2. 3D chemical model of the Ge−Si/Si(001) dome-shaped islands. (A) Perspective top view of the modeled chemical distribution within the island. The line boundaries show the faceted dome, where the facets families (braces) and the directions (brackets) are indicated. (B and C) Side views of the 3D model along the [110] and [100] directions, respectively. This model was constructed assuming a four-fold chemical symmetry. The colors differentiate Ge-rich (reddish) and Si-rich (green) regions. The numbers attributed to each region group refer to specific Ge content ($\%_{atom}$), as indicated by the scale bar.

revealed a good reproducibility for each projection. Moreover, a discerned examination of the HRTEM images and chemical maps was performed to avoid the analysis of severely sectioned or sliced islands originating from specimen preparation (thinning).

The strain maps (Figure 1A and B) shown for the [110] direction are in agreement with what is expected for epitaxial growth and strain relaxation, that is, $\varepsilon_{\parallel} < 0$ and $\varepsilon_{\perp} > 0$, since Ge lattice parameter is larger than Si. The chemical map at the [110] direction (Figure 1C) shows a nonmonotonic behavior along the [001] direction for the Ge distribution ($\%_{atom}$). This projection shows a Ge enrichment at the edges (65 ± 8% Ge), at the core near to the base (70 ± 8% Ge), and at the top (90 ± 8% Ge) of the island, with a region between them with 45 ± 8% Ge. In contrast, Figure 1D ([100] direction) shows a Si enrichment at the edges (28 ± 8% Ge) and a nearly uniform composition at the central area (58 ± 8% Ge), while a high Ge concentration was also found on the top of the islands (90 ± 8% Ge). These features show that the [110] and [100] projections are significantly different and clearly suggest that the Ge arrangement is noncylindrically symmetrical.

The projected chemical maps contrast with previously reported results based on GIXRD measurements[12,13,29] as well as STEM,[10,11] in which a monotonic increase of the Ge concentration from the core to the island shell was observed. These GIXRD studies were performed on the assumption of composition variations only along the growth direction[13,29] or by considering a cylindrical symmetry.[12] On the other hand, selective etching followed by AFM analysis has shown that the composition distribution of such structures may exhibit an angular dependence that breaks the cylindrical symmetry.[8] Here, the 2D chemical maps correspond to the projected average composition at each point, allowing unveiling of noncylindrically symmetric 3D features. Therefore, by using selected projections, one can infer the 3D chemical distribution in a self-consistent fashion. Due to the structural symmetry of the current system, two distinct projections ([110] and [100]) from statistically representative islands were sufficient for performing the 3D reconstruction.

Figure 2 shows a four-fold symmetric model for the Ge and Si distribution, derived from an interpretation of the projected chemical maps and crystal symmetry. Ge−Si islands are multifaceted structures bounded by the {113}, {105}, and {15 3 23} planes,[30] as schematically shown on Figure 2A. The [110] projected chemical map (Figure 1C) suggests a Ge enrichment at the bottom of the {113} facets and at the {105} top facets. Moreover, the [100] chemical map (Figure 1D) indicates a Si-rich region at the bottom of the common edge between the {15 3 23} facets and a Ge enrichment at the {105} top facets.

An algorithm was used to implement this model, which was formed by intersections of different functions, resulting in the structure shown in Figure 2, where constant composition volumes are highlighted in red (Ge-rich) and green (Si-rich). The four-fold 3D model of the island is formed by Ge-enriched regions located by the {113} facets (88% Ge), at the dome top

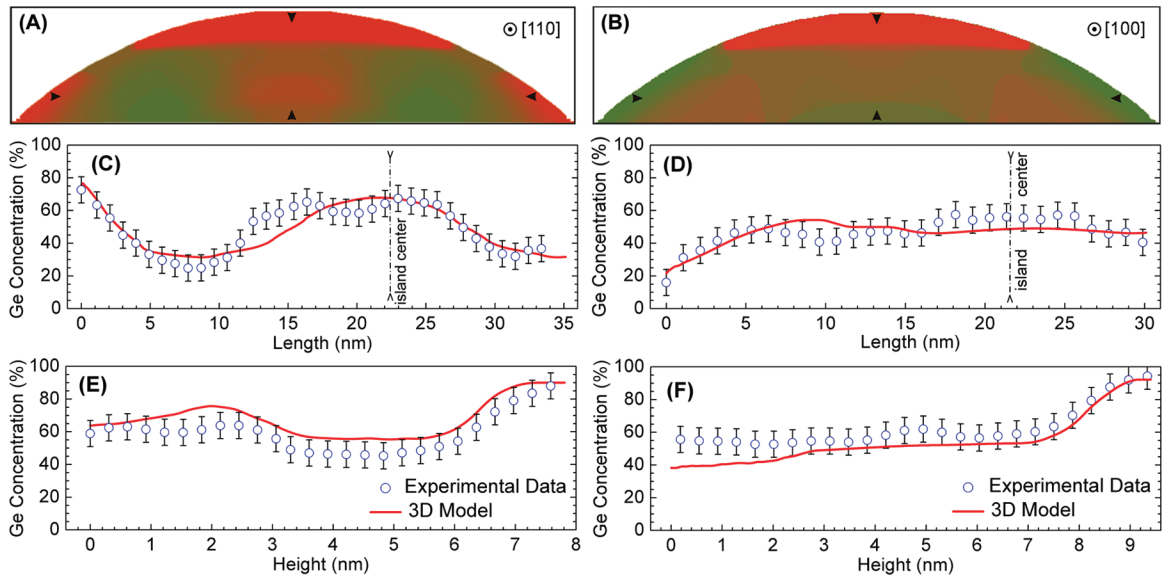

Figure 3. Projected composition maps and line profiles of the 3D model island. (A and B) Projected chemical maps obtained from the 3D proposed model for the [110] and [100] directions, respectively. (C and D) Ge content ($\%_{atom}$) horizontal profiles through a line near to the base (indicated by the arrows) for [110] and [100] directions, respectively. Similarly, (E) and (F) are the Ge concentration vertical profiles taken at the island center, at the positions indicated by the arrows, for [110] and [100] directions, respectively. The solid lines are the profiles obtained from the projected 3D model, and the open circles are the experimental data from the chemical maps shown in Figure 1. The error bars (±8%) were estimated from the standard deviation of the measured compositions at the Si lattice reference.

(90% Ge), and at the island core (75% Ge) and by Si-rich regions by the {15 3 23} facets (25% Ge) and at the base (25% Ge), with the volume among the above parts filled by 50% Ge. This model was used to calculate 2D average projected maps from the [110] and [100] directions, which were compared to the corresponding experimental chemical maps. Such 3D structure was iteratively refined, optimizing shape and composition, resulting in the representation of the chemical arrangement shown in Figure 2. Figure 2B and C shows the perspective view of the modeled island along the [110] and [100] directions, respectively, which are useful to interpret the experimental chemical maps.

Figure 3A and B show the projected maps obtained from the refined model along the [110] and [100] directions. A qualitative visual comparison of these maps with the experimental chemical maps from Figure 1 shows a good agreement. In addition, a quantitative evaluation of the model refinement was conducted using the line profiles shown in Figures 3C and E and 3D and F for [110] and [100] side-views, respectively. The experimental line profiles represent averages taken in a 2 nm width area. An accuracy of ±8% was estimated from the standard deviation of the composition at the Si substrate region. The horizontal Ge concentration profiles (Figure 3C and D) were taken near the island base, and the vertical profiles (Figure 3E and F) were measured at the island center. The experimental data (open circles) are in accordance with the 3D model (solid lines) for both directions, which substantiates the assumption of uniform composition profile ensembles. The vertical Ge variation at the [110] direction, Figure 3E, shows the previously mentioned nonmonotonic profile, which results from the projected 3D chemical distribution. These results highlight the importance of quantitative measurements of 3D composition arrangement of nanostructures, in which complex chemical profiles may be present. Here, an accurate assessment of the composition was achieved by using two different directions, avoiding erroneous conclusions originating from projection artifacts.

In summary, we report a new method that uses HRTEM images to reconstruct the 3D composition arrangement of Ge−Si/Si(001) islands. Composition and strain were self-consistently determined. This methodology stands out as a high spatial resolution tool for obtaining 3D quantitative chemical information, which can be applied to numerous alloyed nanostructured strained crystalline systems.

Acknowledgment. The authors acknowledge LNLS, FAPESP (2007/05165-7), CNPq (382850/2007-6; 152445/2007-2), and HP Brazil for the financial support. G.M.R. acknowledges Dr. T. I. Kamins for kindly supplying the sample utilized in this work.

Supporting Information Available: The theoretical basis with a detailed description of the procedure employed to calculate the chemical and strain maps and a typical reconstructed HRTEM island image. This material is available free of charge via the Internet at http://pubs.acs.org.

References and Notes

(1) Midgley, P. A.; Weyland, M. *Ultramicroscopy* **2003**, *96*, 413–431.
(2) Arslan, I.; Yates, T. J. V.; Browning, N. D.; Midgley, P. A. *Science* **2005**, *309*, 2195–2198.
(3) Li, Z. Y.; Young, N. P.; Di Vece, M.; Palomba, S.; Palmer, R. E.; Bleloch, A. L.; Curley, B. C.; Johnston, R. L.; Jiang, J.; Yuan, J. *Nature* **2008**, *451*, 46–49.
(4) Sadan, M. B.; Houben, L.; Wolf, S. G.; Enyashin, A.; Seifert, G.; Tenne, R.; Urban, K. *Nano Lett.* **2008**, *8*, 891–896.
(5) Jinschek, J. R.; Batenburg, K. J.; Calderon, H. A.; Kilaas, R.; Radmilovic, V.; Kisielowski, C. *Ultramicroscopy* **2008**, *108*, 589–604.
(6) Bimberg, D.; Grundmann, M.; Ledentsov, N. N. *Quantum Dot Heterostructures*; John Wiley & Sons: Chichester, U.K., 1999.
(7) Leite, M. S.; Malachias, A.; Kycia, S. W.; Kamins, T. I.; Williams, R. S.; Medeiros-Ribeiro, G. *Phys. Rev. Lett.* **2008**, *100*, 226101.
(8) Rastelli, A.; Stoffel, M.; Malachias, A.; Merdzhanova, T.; Katsaros, G.; Kern, K.; Metzger, T. H.; Schmidt, O. G. *Nano Lett.* **2008**, *8*, 1404–1409.
(9) Boscherini, F.; Capellini, G.; Di Gaspare, L.; Rosei, F.; Motta, N.; Mobilio, S. *Appl. Phys. Lett.* **2000**, *76*, 682–684.
(10) McDaniel, E. P.; Jiang, Q.; Crozier, P. A.; Drucker, J.; Smith, D. J. *Appl. Phys. Lett.* **2005**, *87*, 223101.
(11) Chaparro, S. A.; Drucker, J.; Zhang, Y.; Chandrasekhar, D.; McCartney, M. R.; Smith, D. J. *Phys. Rev. Lett.* **1999**, *83*, 1199–1202.

(12) Malachias, A.; Kycia, S.; Medeiros-Ribeiro, G.; Magalhães-Paniago, R.; Kamins, T. I.; Williams, R. S. *Phys. Rev. Lett.* **2003**, *91*, 176101.

(13) Schülli, T. U.; Stangl, J.; Zhong, Z.; Lechner, R. T.; Sztucki, M.; Metzger, T. H.; Bauer, G. *Phys. Rev. Lett.* **2003**, *90*, 066105.

(14) Schade, M.; Heyroth, F.; Syrowatka, F.; Leipner, H. S.; Boeck, T.; Hanke, M. *Appl. Phys. Lett.* **2007**, *90*, 263101.

(15) Kret, S.; Ruterana, P.; Rosenauer, A.; Gerthsen, D. *Phys. Status Solidi B* **2001**, *227*, 247–295.

(16) Rosenauer, A. *Transmission Electron Microscopy of Semiconductor Nanostructures: Analysis of Composition and Strain State*; Springer-Verlag, Berlin, Germany, 2003.

(17) Hÿtch, M. J.; Snoeck, E.; Kilaas, R. *Ultramicroscopy* **1998**, *74*, 131–146.

(18) Hÿtch, M. J.; Putaux, J.-M.; Penisson, J.-M. *Nature* **2003**, *423*, 270–273.

(19) Johnson, C. L.; Snoeck, E.; Ezcurdia, M.; Rodríguez-González, B.; Pastoriza-Santos, I.; Liz-Marzán, L. M.; Hÿtch, M. J. *Nat. Mater.* **2008**, *7*, 120–124.

(20) Chung, J.; Rabenberg, L. *Ultramicroscopy* **2008**, *108*, 1595–1602.

(21) Meyer, R. R.; Kirkland, A. I.; Saxton, W. O. *Ultramicroscopy* **2002**, *92*, 89–109.

(22) Hÿtch, M. J.; Plamann, T. *Ultramicroscopy* **2001**, *87*, 199–212.

(23) Hüe, F.; Johnson, C. L.; Lartigue-Korinek, S.; Wang, G.; Buseck, P. R.; Hÿtch, M. J. *J. Electron Microscopy* **2005**, *54*, 181–190.

(24) Kasper, E.; Schuh, A.; Bauer, G.; Hollländer, B.; Kibbel, H. *J. Cryst. Growth* **1995**, *157*, 68–72.

(25) Gschneidner, K. A.; Vineyard, G. H. *J. Appl. Phys.* **1962**, *33*, 3444–3450.

(26) Raiteri, P.; Valentinotti, F.; Miglio, L. *Appl. Surf. Sci.* **2002**, *188*, 4–8.

(27) Seel, S. C.; Thompson, C. V. *J. Appl. Phys.* **2003**, *93*, 9038–9042.

(28) Kamins, T. I.; Carr, E. C.; Williams, R. S.; Rosner, S. J. *J. Appl. Phys.* **1997**, *81*, 211–219.

(29) Magalhães-Paniago, R.; Medeiros-Ribeiro, G.; Malachias, A.; Kycia, S.; Kamins, T. I.; Williams, R. S. *Phys. Rev. B* **2002**, *66*, 245312.

(30) Ross, F. M.; Tromp, R. M.; Reuter, M. C. *Science* **1999**, *286*, 1931–1934.

JP902480W